Aging-Aware Battery Operation for Multicarrier Energy Systems

Slaifstein, Dario; Alpizar Castillo, Joel; Menendez Agudin, Alvaro; Ramirez Elizondo, Laura; Chandra Mouli, Gautham Ram; Bauer, Pavol

Citation (APA)
Slaifstein, D., Alpizar Castillo, J., Menendez Agudin, A., Ramirez Elizondo, L., Chandra Mouli, G. R., & Bauer, P. (2023). Aging-Aware Battery Operation for Multicarrier Energy Systems. In *Proceedings of the IECON 2023- 49th Annual Conference of the IEEE Industrial Electronics Society* (Proceedings of the Annual Conference of the IEEE Industrial Electronics Society). IEEE. https://doi.org/10.1109/IECON51785.2023.10312455

Important note
To cite this publication, please use the final published version (if applicable).
Please check the document version above.

Aging-aware Battery Operation for Multicarrier Energy Systems

Darío Slaifstein
Delft University of Technology
Delft, The Netherlands
D.A.slaifstein@tudelft.nl

Joel Alpízar-Castillo
Delft University of Technology
Delft, The Netherlands
J.J.AlpizarCastillo@tudelft.nl

Alvaro Menendez Agudin
Delft University of Technology
Delft, The Netherlands
A.M.A.Menendezagudin@tudelft.nl

Laura Ramírez-Elizondo
Delft University of Technology
Delft, The Netherlands
L.M.RamirezElizondo@tudelft.nl

Gautham Ram Chandra Mouli
Delft University of Technology
Delft, The Netherlands
G.R.ChandraMouli@tudelft.nl

Pavol Bauer
Delft University of Technology
Delft, The Netherlands
P.Bauer@tudelft.nl

Abstract—In the context of building electrification the operation of distributed energy resources integrating multiple energy carriers poses a significant challenge. Such an operation calls for an energy management system that decides the set-points of the primary control layer in the best way possible. This is done by fulfilling user requirements, minimizing costs, and balancing local generation with energy storage. This last component is what enables building flexibility. This paper presents a novel aging-aware strategy for operating grid-connected buildings that combine multiple energy carriers (heat and electricity), storage devices (electric vehicles, batteries, and thermal storage), and power sources (solar photovoltaics, solar collectors). The novel energy management algorithm presented considers the aging of the batteries to enhance the operational differences between storage technologies, thus making explicit the trade-off between the services provided by the hybrid energy storage system and its degradation. This unlocks grid cost reductions between 20-45% depending on the season when compared to state-of-the-art solutions.

Index Terms—Energy management systems, Battery degradation, Hybrid energy storage, Multicarrier energy systems

I. INTRODUCTION

Economic decarbonization is a significant challenge for modern societies. In particular, the sustainable transformation of both the power and transport sectors poses substantial technical and cultural challenges [1]. Both transitions couple in the population's homes where electricity, mobility, or HVAC are needed. Thus, possible synergies between the three systems can be exploited to achieve the desired decarbonization, freedom, resiliency, and cost savings [2]. The successful exploitation of such coupling needs to be carefully tailored and built into the design of modern multicarrier energy systems (MCES) [2]–[10]. This necessarily leads to advanced energy management systems (EMS) that schedule and control the distributed energy resources (DER)s [5], [6], [9], [11]–[13]. The EMS needs to handle uncertain and variable forecasts
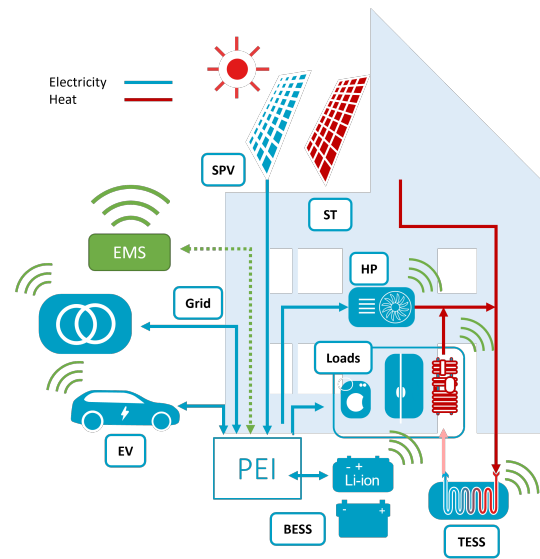
Fig. 1: Schematic diagram of the proposed electrified multi-carrier building.

(electric vehicles [14], solar, loads), aging storage assets (batteries [15]–[19]), and user preferences.

To dispatch and operate such systems, the literature suggests different methods such as stochastic optimization [20], reinforcement learning (RL) [6], [7], [9], Model Predictive Control (MPC) [4]–[6], [11], [12], and many others. Stochastic optimization requires precise characterization of the scenarios to be simulated, and it incurs heavy computations. The high computational cost is either because it needs to run several sampled scenarios (Monte Carlo method), or non-linear distributions must be propagated along the whole simulation window. RL approaches have challenges in maintaining robustness under unknown situations, are sometimes non-interpretable, difficult to tune its parameters, and do not necessarily follow physical constraints, even when a model-based RL is used [6], [7], [9]. Finally, MPC appears as one of the most popular methods

in the literature [6]. In it, the optimal controller contains domain-based models of the system dynamics and uses them to construct the optimal trajectories for the current time step. The controller handles uncertainty and real-time operation by moving the time window of that time-step optimization, updating the states with measurements and forecasts, and using accurate models. The main advantage is that decisions are traceable, the trade-offs explicit, and design limits and physical constraints can be integrated easily. All methods need extensive hyper-parameter tuning, and safeguarding optimality conditions to be implemented.

The energy storage systems (ESS) technologies, such as Li-ion batteries (LIB) and electric vehicles (EV), are limited by their aging [5], [16]–[19], [21], [22], as well as by their availability for mobility in the case of the EVs [14], [22]. The combination of different ESS technologies is a powerful tool for securing the energy supply in a safe, cost-effective, and reliable manner [23], [24]. However, the operation of such systems is still an open question because of their different carriers, dynamics, efficiencies, and costs. Moreover, even though battery aging mechanisms have been studied and modeled extensively at the battery management systems (BMS) level, this has not been incorporated into the design of an EMS with multiple energy vectors [5], [22]. This is because such degradation mechanisms introduce non-linear models, increasing the overall complexity.

The contribution of this paper is an aging-aware strategy operation that exploits the trade-off between battery operation and its degradation in the context of energy systems with multiple carriers. Our strategy is an optimization-based secondary controller that minimizes energy cost and battery aging. A schematic of such a system is presented in Fig. 1. The system is composed of solar photovoltaics (SPV), battery energy storage system (BESS),EV, power electronic interface (PEI), heat pump (HP), solar thermal (ST), thermal energy storage system (TESS), grid connection and loads. The EMS makes a clear distinction between fast (electrical) and slow (thermal) ESS, crucial to designing MCES. Despite two ESS might have the same performance ratings, their dynamics and technologies are fundamentally different; therefore, the controller has to account for it.

II. MODELING & ALGORITHMS

The following section describes the models included in the EMS. The modeling is done following the Universal Modeling Framework (UMF) by Powell [25]–[27].

The EMS plans a day ahead operation, considering perfect information where the sizing of the components is known. Hence, the costs of the system are only its operation costs. These are the net grid cost C_{grid} and the battery degradation cost C_{loss}. Lastly, to account for the user's mobility requirement, a fictitious penalty p_{SoCDep} is incorporated to quantify possible deviations from the desired SoC of the EV

at departure. The optimization problem is then reduced to

$$
\begin{aligned}
\min_{P_{a,t}^*} \quad & C_{\text{grid}} + p_{\text{SoCDep}} + C_{\text{loss}} \\
\text{s.t.} \quad & S_{a,t+1} = S_{a,t}^M(S_{a,t}, P_{a,t}^*, W_{t+1}|\theta_{a,t}) \\
& P_{a,t}^* = X^\pi(S_{a,t}) \in \mathcal{P} \qquad \forall a \in \mathbb{A} \\
& S_{a,t} \in \mathcal{S} \qquad\qquad\quad \forall a \in \mathbb{A}
\end{aligned} \quad (1)
$$

with

$$
a = \{\text{SPV}, \text{grid}, n_{\text{EV}}, \text{BESS}, \text{HP}, \text{ST}, \text{TESS}\}. \quad (2)
$$

The components of the objective are

$$
C_{\text{grid}} = w_{\text{grid}} \sum_0^T \lambda_{\text{buy}}.P_{\text{grid}}^+ + \lambda_{\text{sell}}.P_{\text{grid}}^-.\Delta t, \quad (3)
$$

$$
p_{\text{SoCDep}} = w_{\text{SoC}}.||\varepsilon_{\text{SoC}}||_2^2, \quad (4)
$$

and

$$
C_{\text{loss}} = w_{\text{loss}}.c_{\text{loss}}.\sum_0^T \sum_{sa} i_{\text{loss}}.\Delta t, \ \forall \ sa \subset a, \quad (5)
$$

where $S_{a,t}$ is the state vector, $P_{a,t}^*$ is the optimal decision for timestep t, W_{t+1} is an exogenous process that introduces new information after making a decision. The mappings $S_{a,t}^M(.)$, and $X^\pi(.)$ are the transition function and optimal policy, respectively. The first is a set of equations describing the states and parameter evolution, and the second is the algorithm that finds the optimal setpoints. The vector $\theta_{a,t}$ contains all the parameters of each asset a and changes over time t. The subindex $a \in \mathbb{A}$ corresponds to the assets shown in Fig. 1 which are PV panels, grid connection, electric vehicles, stationary battery, heat pump, solar thermal system and thermal storage. Additionally, $sa = \{\text{BESS}, n_{\text{EV}}\} \subset a$ denotes the electric storage assets and $n_{\text{EV}} = 1...N_{\text{EV}}$ is the number of EV. The time window is $T = 24$ hr and the timestep $\Delta t = 15$min. The three components of the objective function are the grid cost C_{grid}, the cost of lost energy capacity C_{loss}, and a penalty for not charging the EV to the desired setpoint p_{SoCDep}. C_{loss} is explained in Section II-A2.

The following definitions of the elements are considered:
- The state vector is

$$
S_{a,t} = [P_{\text{PV}}, P_{\text{grid}}, \gamma_{n_{\text{EV}}}, P_{\text{HP}}^{\text{e}}, P_{\text{HP}}^{\text{th}}P_{\text{ST}}, P_{\text{load}}^{\text{e}}, P_{\text{load}}^{\text{th}}]_t^T.
$$

where $P_{a,t}$ is the power of the assets and $\gamma_{n_{\text{EV}}}$ is the EV availability
- The policy or decision variables are

$$
P_{a,t}^* = [P_{n_{\text{EV}}}, P_{\text{BESS}}, P_{\text{TESS}}]_t^T.
$$

- The superscripts e and th refer to electricity or thermal carriers. They are used when the subscript is the same.
- Both the policy and state vectors have upper and lower limits denoted as $\overline{P}_{a,t}^*$, $\underline{P}_{a,t}^*$, $\overline{S}_{a,t}$, and $\underline{S}_{a,t}$.
- All bidirectional variables, either policies or states, are modeled with two constraints:

$$
S_t^+ + S_t^- = S_t \wedge \ S_t^- \leq 0, S_t^+ \geq 0, \quad (6)
$$

and

$$S_t^+ . S_t^- = 0 \qquad (7)$$

- Uncertainty is tackled through a direct-lookahead policy (DLA) $X^\pi(.)$ in a deterministic setup where at each timestep t we take the median of a forecast $W_{t+1} = 0$. In our case, our policy mapping is our optimization algorithm.
- The order of the subscript is *"name, device, time index"*.
- Capital C denotes total cost in €, lowercase c denotes unit cost and w indicates tunning/scaling weight.

The inputs of the operation are the solar power P_{PV}, the prices $\lambda_{\text{buy/sell}}$, the electric demand $P_{\text{load}}^{\text{e}}$, and the thermal demand $P_{\text{load}}^{\text{th}}$.

To define transition function $S_{a,t}^M(.)$ all assets need to be modeled. The thermal assets are incorporated with the following linear models:

$$P_{\text{HP}}^{\text{th}} = \eta_{\text{HP}} . P_{\text{HP}}^{\text{e}} , \qquad (8)$$

$$P_{\text{ST}} = \eta_{\text{ST}} . P_{\text{PV}} , \qquad (9)$$

and

$$SoC_{\text{TESS},t+1} = SoC_{\text{TESS},t} - \frac{\Delta t}{Q_{\text{TESS}}.3600} . \eta_{\text{TESS}} . P_{\text{TESS},t} , \qquad (10)$$

where η denotes a conversion factor or efficiency, Q_{TESS} is the capacity in kWh. The thermal balance comes in as:

$$P_{\text{ST}} + P_{\text{HP}}^{\text{th}} + P_{\text{TESS}} = P_{\text{load}}^{\text{th}} . \qquad (11)$$

The electric power balance, on the other hand, is

$$P_{\text{PV}} + P_{\text{BESS}} + \sum_{n_{\text{EV}}=1}^{N_{\text{EV}}} \gamma_{n_{\text{EV}}} . P_{n_{\text{EV}}} + P_{\text{grid}} = P_{\text{load}}^{\text{e}} + P_{\text{HP}}^{\text{e}} . \qquad (12)$$

where $\gamma_{n_{\text{EV}}}$ is the EV availability, explained in Section II-B.

A. Electric storage modeling

This subsection describes the models used to describe the performance and degradation of the electric storage denoted by sa. The performance model $S_{sa,t}^M(.)$ describes the evolution of the states $S_{sa,t}$, and the degradation model $g_{sa,t}(.)$ describes the dynamics of the parameters $\theta_{sa,t}$ that parameterize the performance model. These performance and aging sub-models are part of the main transition function $S_{a,t}^M(.)$.

1) Performance models:
Bucket model (BM)

A basic model of the operation of a battery assumes that its output voltage v_t is linear with the state of charge SoC, assuming no voltage drop. Hence the only equations of this model are

$$SoC_{sa,t+1} = SoC_{sa,t} - \frac{\Delta t}{Q_{sa,t}.3600} . \eta_c . i_{sa,t} , \qquad (13)$$

$$i_{sa,t} = \frac{P_{sa,t}}{v_{sa,t} . N_{s,sa} . N_{p,sa}} , \qquad (14)$$

and

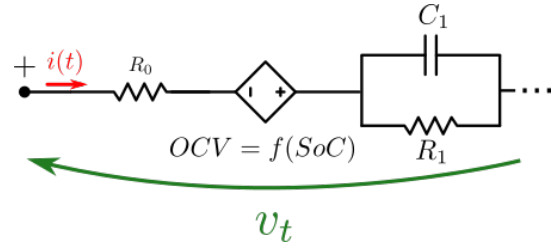$$OCV_{sa,t} = a_{OCV,sa} + b_{OCV,sa} . SoC_{sa,t} , \qquad (15)$$

Fig. 2: First order Equivalent Circuit Model.

$$v_{t,sa,t} = OCV_{sa,t} , \qquad (16)$$

where $i_{sa,t}$ is the current passing through the cell, $OCV_{sa,t}$ is the open circuit voltage, $a_{OCV,sa}$ and $b_{OCV,sa}$ are the voltage model parameters, η_c is the Coulombic efficiency and $Q_{sa,t}$ is the cell capacity in Ah. Each battery pack is assumed to be organized as a Series Cell Module (SCM) where $N_{s/p,\ sa}$ are the series and parallel cells and branches, respectively.

Equivalent Circuit Model (ECM)

To improve the accuracy of the model, a first order Equivalent Circuit Model (ECM) can be incorporated, as in Fig. 2. The performance sub-model $S_{sa,t}^M(.)$ is then modified with:

$$i_{R_1,sa,t+1} = e^{\frac{\Delta t}{R_{1,sa} . C_{1,sa}}} . i_{R_1,sa,t} + \left(1 - e^{\frac{\Delta t}{R_{1,sa} . C_{1,sa}}} \right) . i_{sa,t} \qquad (17)$$

$$v_{sa,t} = OCV_{sa,t} - i_{R_1,sa,t} . R_{1,sa} - i_{sa,t} . R_{0,sa} , \qquad (18)$$

where $i_{R_1,sa,t}$ is the pole current, $R_{1,sa}$ and $C_{1,sa}$ are the pole elements and $R_{0,sa}$ is the series resistance as defined in Fig. 2. Eqs. 13, 14 and 15 are maintained. The ECM incorporates the series voltage drop ($R_{0,sa}$) that limits power output and the first-order diffusion dynamics ($R_{1,sa}$ and $C_{1,sa}$). This sub-model further differentiates electric and thermal ESS technologies.

2) Empirical degradation model $g_{sa,t}(.)$: The degradation model follows the work from Wang et al. [28], which summarizes all aging mechanisms into calendar (i_{cal}) and cyclic (i_{cycle}) aging currents. The chosen degradation model only describes the capacity fade, neglecting the power fade. Its equations are:

$$i_{\text{cycle},sa,t} = \frac{c_1 . c_3}{c_4} . e^{c_2 . |i_{sa,t}|} . (1 - SoC_{sa,t}) . |i_{sa,t}| , \qquad (19)$$

$$i_{\text{cal},sa,t} = c_5 . e^{-\frac{24\,\text{kJ}}{RT}} . \sqrt{t} , \qquad (20)$$

$$i_{\text{loss},sa,t} = i_{\text{cycle},sa,t} + i_{\text{cal},sa,t} , \qquad (21)$$

and

$$Q_{sa,t+1} = Q_{sa,t} - \frac{\Delta t}{3600} . i_{\text{loss},sa,t} . \qquad (22)$$

where $c_{1:5}$ are empirical parameters coming from curve fitting [28], R is the gas constant and T is the temperature.
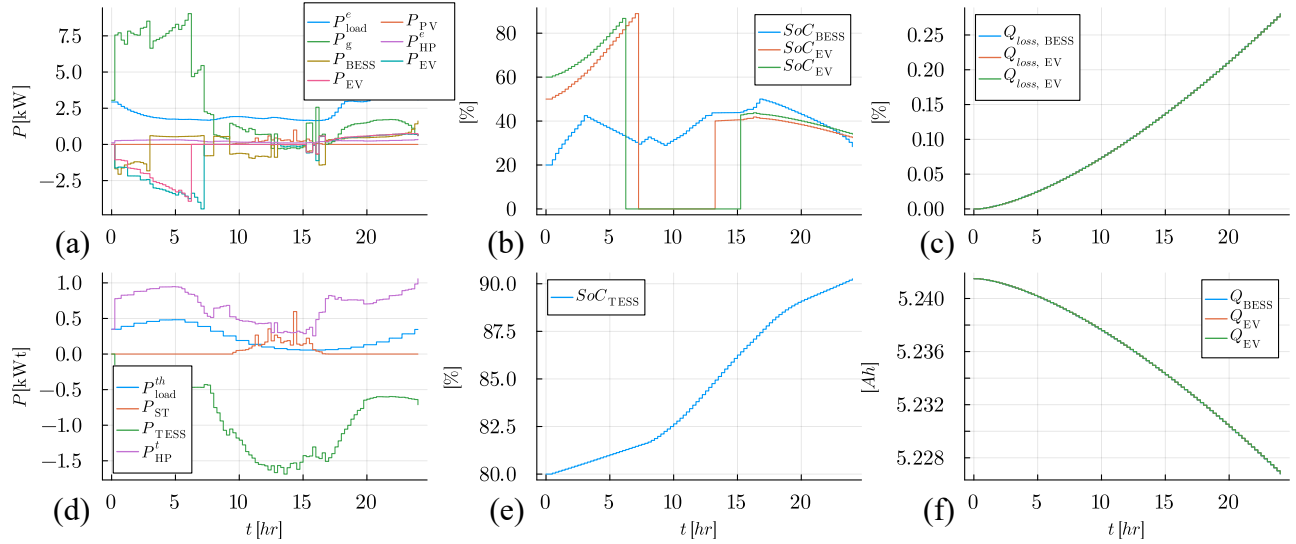
Fig. 3: Dashboard for *CEmpDeg* EMS for a typical summer day of 2022. a) Electric balance. b) Electric storage. c) Relative lost capacity. d) Thermal balance. e) Thermal storage. f) Total cell capacity.

TABLE I: Parameters for the empirical degradation model [28]

Parameter	Value
c_1	0.0008
c_2	0.39
c_3	1.035
c_4	50
c_5	1.721×10^{-4}

B. Electric Vehicles

From the point of view of a residential building, the EVs are a BESS with availability constraints and certain requirements regarding their SoC at departure time t_{dep}. For the availability γ, the probability distributions of departure (t_{dep}) and arrival (t_{arr}) times can be described as random variables with Gaussian distributions $t_{\text{dep/arr}} \sim \mathcal{N}(\mu_{\text{dep/arr}}, \sigma^2_{\text{dep/arr}})$. The availability γ_t will then be

$$\gamma_t = \begin{cases} 0 & t \in [t_{\text{dep}};\ t_{\text{arr}}] \\ 1 & \text{otherwise} \end{cases}. \tag{23}$$

The power balance of an EV is

$$P_{tot,n_{\text{EV}},t} = \gamma_{n_{\text{EV}},t}.P_{n_{\text{EV}},t} + (1 - \gamma_{n_{\text{EV}},t}).P_{\text{drive},n_{\text{EV}}}, \tag{24}$$

where $P_{\text{tot},n_{\text{EV}},t}$ is the total power of the EV, $P_{n_{\text{EV}},t}$ is the charger power, and $P_{\text{drive},n_{\text{EV}}}$ is the power consumed driving assuming no public charging. The total power $P_{\text{tot},n_{\text{EV}},t}$ is then used in (14) and later for calculating the aging of the EV batteries. The average driving power is also sampled from a Gaussian distribution $P_{\text{drive},n_{\text{EV}}} \sim \mathcal{N}(\mu_{\text{drive}}, \sigma^2_{\text{drive}})$.

Additionally, the EV is required to be delivered with a minimum SoC as

$$SoC_{EV}(t_{\text{dep}}) = SoC_{\text{dep}}. \tag{25}$$

This is implemented as a penalty in the cost function (soft constraint) since an equality constraint might be too strict and cause non-convergence. This extra cost is defined by taking
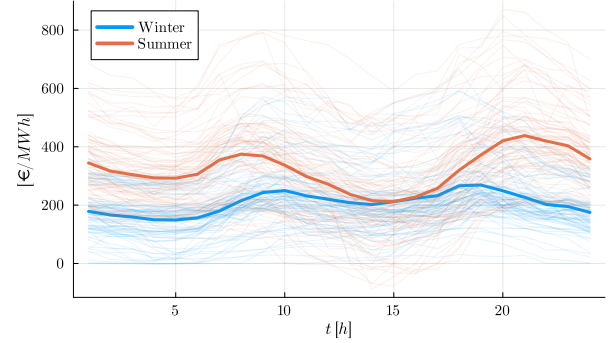

Fig. 4: EPEX day-ahead auction prices for summer and winter. The bold lines show the mean hourly prices.

the squared L2 norm of the deviation ε_{SoC}, from Eq.4, and defined as:

$$\varepsilon_{\text{SoC}} = SoC_{EV}(t_{\text{dep}}) - SoC_{\text{dep}}, \tag{26}$$

III. CASE STUDY & RESULTS

To assess the performance of incorporating aging into the MCES operation, our proposed controller is benchmarked against a controller without a degradation sub-model. The first controller will be called "*CEmpDeg*" and contains a first-order ECM with an Empirical aging model. The second controller, called "*BNoDeg*" has a bucket model without an aging model, Eqs. 19 - 22. The two controllers are compared for the Netherlands' typical summer and winter days in 2022. Even though their objective functions and constraints/models are different, the final informed results are calculated with the full objective function presented in Eq.1. This means that for the "*BNoDeg*" controller the created power setpoints are used to calculate C_{loss}.

$w = [w_{\mathrm{grid}}, w_{\mathrm{EVs}}, w_{\mathrm{loss}}]^T$				
	summer		Winter	
Weight	*CEmpDeg*	*BNoDeg*	*CEmpDeg*	*BNoDeg*
w_{grid}	1000	1000	1000	500
w_{EVs}	1000	1000	1000	1000
w_{loss}	600	0	600	0

TABLE II: Objective function weights.

The system is composed of a 5kWp SPV, a 20kWh BESS with LFP cells, two 12.5kW EV charging points, a 4kWe heat pump, a 2.7kWth solar thermal collector, a 200kWh TESS, a 6kWp electrical load, a 1kWp thermal demand, and 10kW LV grid connection.

The output of the SPV is taken from [29]–[31], the market prices λ are taken from the EPEX day-ahead auction, shown in Fig.4, and $\lambda_{\mathrm{buy}} = 0.95\lambda_{\mathrm{sell}}$ [32], the power demand was modeled taking the standard consumption patterns [33], and the heat demand was modeled as [34]. The $g_{sa,t}(.)$ model is parameterized for LIB cells with Nickel manganese cobalt oxide (NMC) cathodes and graphite anodes, model parameters are presented in Table I. The sampling time is $\Delta t = 15$ min, and the total number of EVs is $N_{\mathrm{EV}} = 2$.

In this case study, the weights w used for the objective function $C(S_t, P_t)$ are presented in Table II. The w is chosen for regularization purposes and tunning preferences. Hence the user has direct control over how the controller behaves by changing the ratio between w_{grid} and w_{loss}. Additionally, the reader has to remember that the submodels used for the performance $S_{sa}^M(.)$ and the aging $g_{sa}(.)$ are different between the controllers.

Our optimization algorithm result in the optimal scheduling of the power dispatch P_t^*. The optimal day-ahead strategy of the *CEmpDeg* controller is shown in Fig. 3 for the typical summer day. The dashboard presents the electric power and thermal balances, the SoC of the storage devices, and the evolution of the capacities Q_{sa}. Figs. 3a and 3d present the P_t^* for the electric and thermal carriers. Given the signal prices and the high solar generation for this typical summer day the highest electric load is the EV charging requirement at the beginning of the day. For the thermal carrier, the controller chooses to charge the TESS taking advantage of low prices of the first half of the day. The heat pump follows the thermal load and ramps down when solar heat generation occurs. The excess heat from the heat pipes charges the TESS. In this sense, for the chosen sizing the TESS is not used for daily variations. Further evidence is needed to quantify the impact of BESS modeling in its weekly and/or seasonal operation.

As for the battery aging, Figs.3c and 3f, the total degradation $Q_{\mathrm{loss},\ sa}$ is less than 0.3 % per cell. In this work, it is assumed that all cells are identical and hence their aging parameters are the same, thus their only difference would come from their utilization. Unfortunately, for the given 24h period and set of initial parameters calendar aging is 2 orders of magnitude higher than cyclic aging, in accordance to [28]. Since cyclic aging represents the operation of the batteries, there's no significant difference between Q_{sa}.

The key difference between controllers is how they use electric storage, Fig. 5. In the *CEmpDeg* controller, the sa are used more aggressively (understanding this as higher peak power values) during the summer to achieve higher earnings, Fig. 5a. On the other hand for winter, Fig.5b, the P_{sa}^* better captures marginal prices. The results show how the EVs are not available during $t \in [t_{\mathrm{dep}}, t_{\mathrm{arr}}]$; nevertheless, they are used for bidirectional power when connected. The long-duration thermal storage stays mostly idle during the day, only changing 10-15% in both seasons. The algorithm also successfully distinguishes between the fast dynamics of electrical storage and the slow dynamics of the TESS. Using the fast dynamics of the LIBs to balance out hourly and daily variations. This also impacts the operation of the TESS presented in Figs. 5c and 5d. In the *CEmpDeg* the SoC deviation of the thermal buffer is slightly less when compared to *BNoDeg*.

Finally, for the typical days analyzed, Fig. 6 presents the cumulative grid cost C_{grid} curves. The results confirmed that enhancing the models used for the batteries allows a more aggressive strategy that pays off with 22% and 48% cost reductions for summer and winter, respectively. Additionally, calendar aging dominates by almost 2 orders of magnitude over cyclic aging, thus the difference in Q_{loss} between "CEmpDeg" and "BNoDeg" is negligible (less than 0.3mAh/day per cell). This is why the change in objective function and constraints enables better grid costs C_{grid}. Since the total capacity fade is going to remain the same for both algorithms the aging submodel enhances the decisions taken by the "CEmpDeg" . Of course, this is a direct consequence of the period being simulated. For longer simulation times this would not necessarily hold and the trade-off between degradation and grid operation should be controlled by tunning w. Further research is needed to clarify this point.

IV. CONCLUSIONS

In the context of designing EMS algorithms for multicarrier energy systems, this paper showed how the proposed aging-aware operation strategy enables 20-45% grid cost (C_{grid}) reductions without significant differences in lost battery capacity (Q_{loss}). This is achieved by enhancing the controller's battery models with equivalent circuits and empirical aging models. An explicit trade-off between battery operation and its degradation is considered, hence improving the C_{grid} for the user. At the same time, the user requirements ($P_{\mathrm{load}}^{\mathrm{e/th}}$ and SoC_{dep}) are successfully fulfilled.

Another difference between the two controllers is the TESS operation, shown in Figs.5c and 5d. This displays how the operation between carriers is related. Unfortunately, this relationship depends on system sizing, thus further evidence is needed to clearly define its scope and impact.
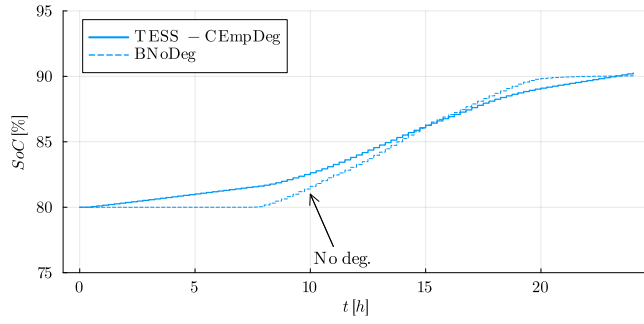
Further works include the expansion of the performance and degradation sub-models with physics-based models [15], [16], [18], [21], [35]–[39]. Such models have extrapolating characteristics, which is not the case with the empirical aging model used in this work. Empirical models that aggregate different degradation mechanisms into calendar and cyclic
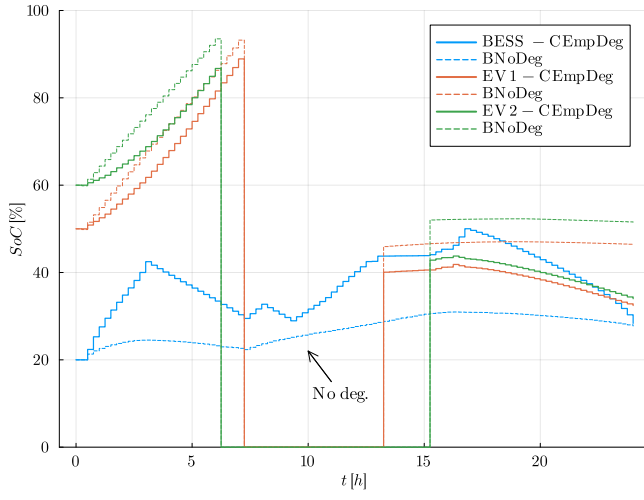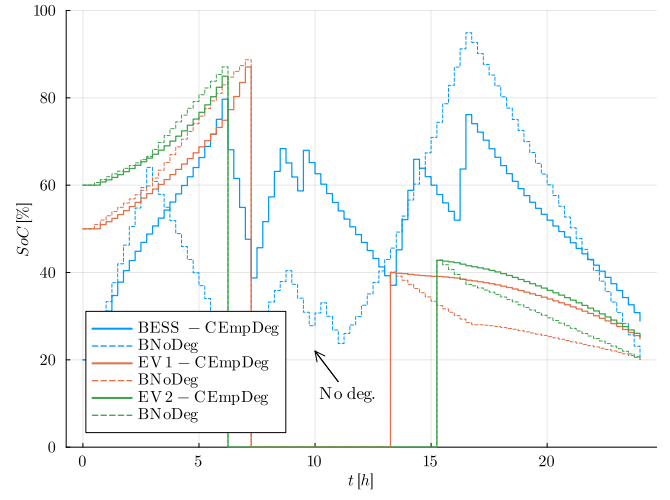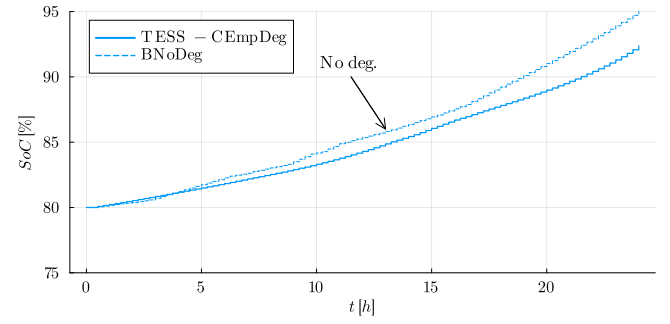
Fig. 5: a) Electrical storage for a typical summer day, b) winter day, c) TESS for a typical summer day, d) winter day.

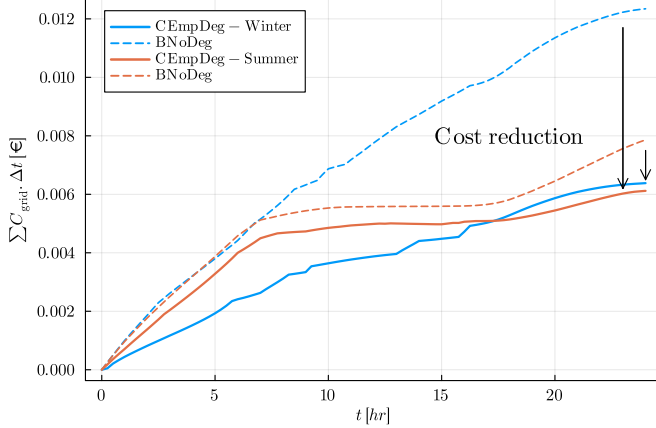Fig. 6: Cumulative grid cost C_{grid} for typical summer and winter days.

aging do not reflect varying operating conditions. Another way to go is to move from a static policy to an adaptive policy ($X^\pi \rightarrow X_t^\pi$) to naturally handle the changes both in the parameters $\theta_{a,t}$ as well as the belief states $B_{a,t}$. The latter encloses information on the different sources of uncertainty in the problem, which change in real-time as the system operates. Finally, the relationship between the carriers has to be further explored with more extensive simulation and experimental work showing intraday, weekly and seasonal operation of the MCES.

REFERENCES

[1] IEA, "Net Zero by 2050: A Roadmap for the Global Energy Sector," *International Energy Agency*, p. 224, 2021.

[2] M. Geidl and G. Andersson, "Optimal Power Flow of Multiple Energy Carriers," *IEEE Transactions on Power Systems*, vol. 22, no. 1, pp. 145–155, 2 2007. [Online]. Available: https://ieeexplore.ieee.org/document/4077107/

[3] G. Andersson, E. Zurich, and M. Geidl, "Optimal power dispatch and conversion in systems with multiple energy carriers plangridev view project bpes-optimal sizing and control of balancing power in the future eu power system considering transmission constraints view project optimal power dispatc," *Proceedings 15th Power Systems Computation Conference (PSCC).*, 2005, fundamental pioneering paper. [Online]. Available: https://www.researchgate.net/publication/228776936

[4] W. Vermeer, G. R. C. Mouli, and P. Bauer, "Real-Time Building Smart Charging System Based on PV Forecast and Li-Ion Battery Degradation," *Energies 2020, Vol. 13, Page 3415*, vol. 13, no. 13, p. 3415, 7 2020. [Online]. Available: https://www.mdpi.com/1996-1073/13/13/3415

[5] ——, "Optimal Sizing and Control of a PV-EV-BES Charging System Including Primary Frequency Control and Component Degradation," *IEEE Open Journal of the Industrial Electronics Society*, vol. 3,

pp. 236–251, 3 2022. [Online]. Available: https://ieeexplore.ieee.org/document/9740621/

[6] G. Ceusters, R. C. Rodríguez, A. B. García, R. Franke, G. Deconinck, L. Helsen, A. Nowé, M. Messagie, and L. R. Camargo, "Model-predictive control and reinforcement learning in multi-energy system case studies," *Applied Energy*, vol. 303, p. 117634, 12 2021. [Online]. Available: https://linkinghub.elsevier.com/retrieve/pii/S0306261921010011

[7] G. Ceusters, L. R. Camargo, R. Franke, A. Nowé, and M. Messagie, "Safe reinforcement learning for multi-energy management systems with known constraint functions," *Energy and AI*, vol. 12, p. 100227, 4 2023. [Online]. Available: https://www.sciencedirect.com/science/article/pii/S2666546822000738

[8] D. Van Der Meer, G. R. C. Mouli, G. M. E. Mouli, L. R. Elizondo, and P. Bauer, "Energy Management System with PV Power Forecast to Optimally Charge EVs at the Workplace," *IEEE Transactions on Industrial Informatics*, vol. 14, no. 1, pp. 311–320, 1 2018.

[9] Y. Ye, D. Qiu, X. Wu, G. Strbac, and J. Ward, "Model-Free Real-Time Autonomous Control for a Residential Multi-Energy System Using Deep Reinforcement Learning," *IEEE Transactions on Smart Grid*, vol. 11, no. 4, pp. 3068–3082, 7 2020. [Online]. Available: https://ieeexplore.ieee.org/document/9016168/

[10] R. Li, A. J. Satchwell, D. Finn, H. Christensen, M. Kummert, J. Le Dréau, R. A. Lopes, H. Madsen, J. Salom, G. Henze, and K. Wittchen, "Ten questions concerning energy flexibility in buildings," *Building and Environment*, vol. 223, p. 109461, 2022. [Online]. Available: https://www.sciencedirect.com/science/article/pii/S0360132322006928

[11] W. Vermeer, G. R. Chandra Mouli, and P. Bauer, "A Multi-Objective Design Approach for PV-Battery Assisted Fast Charging Stations Based on Real Data," *2022 IEEE Transportation Electrification Conference and Expo, ITEC 2022*, pp. 114–118, 2022.

[12] A. Esmaeel Nezhad, A. Rahimnejad, P. H. J. Nardelli, S. A. Gadsden, S. Sahoo, and F. Ghanavati, "A Shrinking Horizon Model Predictive Controller for Daily Scheduling of Home Energy Management Systems," *IEEE Access*, vol. 10, pp. 29 716–29 730, 2022. [Online]. Available: https://ieeexplore.ieee.org/document/9732346/

[13] J. Alpízar-Castillo, L. Ramirez-Elizondo, and P. Bauer, "Assessing the role of energy storage in multiple energy carriers toward providing ancillary services: A review," *Energies*, vol. 16, no. 1, 2023. [Online]. Available: https://www.mdpi.com/1996-1073/16/1/379

[14] P. Alexeenko and E. Bitar, "Achieving reliable coordination of residential plug-in electric vehicle charging: A pilot study," *Transportation Research Part D: Transport and Environment*, vol. 118, p. 103658, 5 2023.

[15] M. A. Xavier, A. K. de Souza, K. Karami, G. L. Plett, and M. S. Trimboli, "A Computational Framework for Lithium Ion Cell-Level Model Predictive Control Using a Physics-Based Reduced-Order Model," *IEEE Control Systems Letters*, vol. 5, no. 4, pp. 1387–1392, 10 2021. [Online]. Available: https://ieeexplore.ieee.org/document/9259035

[16] X. Jin, "Aging-Aware optimal charging strategy for lithium-ion batteries: Considering aging status and electro-thermal-aging dynamics," *Electrochimica Acta*, vol. 407, p. 139651, 3 2022. [Online]. Available: https://linkinghub.elsevier.com/retrieve/pii/S0013468621019356

[17] Y. Li, Y. Yang, J. Tang, B. Xiong, X. Deng, and D. Tang, "Design of Degradation-Conscious Optimal Dispatch Strategy for Home Energy Management System With Rooftop PV and Lithium-Ion Batteries," in *2019 4th International Conference on Intelligent Green Building and Smart Grid (IGBSG)*. IEEE, 9 2019, pp. 741–746. [Online]. Available: https://ieeexplore.ieee.org/document/8886194/

[18] G. L. Plett, *Battery Management Systems Volume I Battery Modeling*. Artech House Power Engineering and Power Electronics, 2015. [Online]. Available: https://us.artechhouse.com/Battery-Management-Systems-Volume-1-Battery-Modeling-P1752.aspx

[19] ——, *BATTERY MANAGEMENT SYSTEMS Volume II: Equivalent-Circuit Methods*, 1st ed. Artech House Power Engineering and Power Electronics, 2016. [Online]. Available: https://ieeexplore.ieee.org/document/9100098

[20] Z. Chen, L. Wu, Y. Fu, Z. Chen, and L. Wu, "Real-Time Price-Based Demand Response Management for Residential Appliances via Stochastic Optimization and Robust Optimization Sets and Parameters," *IEEE Transactions on Smart Grid*, vol. 3, 2012.

[21] J. M. Reniers, G. Mulder, and D. A. Howey, "Review and Performance Comparison of Mechanical-Chemical Degradation Models for Lithium-Ion Batteries," *Journal of The Electrochemical Society*, vol. 166, no. 14, pp. A3189–A3200, 9 2019. [Online]. Available: https://iopscience.iop.org/article/10.1149/2.0281914jes

[22] W. Vermeer, G. R. Chandra Mouli, and P. Bauer, "A Comprehensive Review on the Characteristics and Modeling of Lithium-Ion Battery Aging," *IEEE Transactions on Transportation Electrification*, vol. 8, no. 2, pp. 2205–2232, 6 2022. [Online]. Available: https://ieeexplore.ieee.org/document/9662298/

[23] D. Zhang, N. Shah, and L. G. Papageorgiou, "Efficient energy consumption and operation management in a smart building with microgrid," *Energy Conversion and Management*, vol. 74, pp. 209–222, 10 2013.

[24] M. Aneke and M. Wang, "Energy storage technologies and real life applications – A state of the art review," *Applied Energy*, vol. 179, pp. 350–377, 2016. [Online]. Available: http://dx.doi.org/10.1016/j.apenergy.2016.06.097

[25] W. B. Powell, "A unified framework for stochastic optimization," *European Journal of Operational Research*, vol. 275, no. 3, pp. 795–821, 6 2019.

[26] ——, *Sequential Decision Analytics and Modeling Modeling with Python*. Now Foundations and Trends, 2022.

[27] I. Halperin, "Reinforcement Learning and Stochastic Optimization: A Unified Framework for Sequential Decisions," *Quantitative Finance*, vol. 22, no. 12, pp. 2151–2154, 12 2022. [Online]. Available: https://www.tandfonline.com/doi/full/10.1080/14697688.2022.2135456

[28] J. Wang, J. Purewal, P. Liu, J. Hicks-Garner, S. Soukazian, E. Sherman, A. Sorenson, L. Vu, H. Tataria, and M. W. Verbrugge, "Degradation of lithium ion batteries employing graphite negatives and nickel–cobalt–manganese oxide + spinel manganese oxide positives: Part 1, aging mechanisms and life estimation," *Journal of Power Sources*, vol. 269, pp. 937–948, 12 2014. [Online]. Available: https://linkinghub.elsevier.com/retrieve/pii/S037877531401074X

[29] A. Smets, K. Jäger, O. Isabella, R. van Swaaij, and M. Zeman, *Solar Energy: The physics and engineering of photovoltaic conversion, technologies and systems*. UIT Cambridge Ltd, 2016. [Online]. Available: https://ebookcentral-proquest-com.tudelft.idm.oclc.org/lib/delft/detail.action?docID=4781743

[30] I. Diab, B. Scheurwater, A. Saffirio, G. R. Chandra-Mouli, and P. Bauer, "Placement and sizing of solar PV and Wind systems in trolleybus grids," *Journal of Cleaner Production*, vol. 352, p. 131533, jun 2022.

[31] I. Diab, A. Saffirio, G. R. Chandra-Mouli, and P. Bauer, "A simple method for sizing and estimating the performance of PV systems in trolleybus grids," *Journal of Cleaner Production*, vol. 384, p. 135623, jan 2023.

[32] "EPEX Spot," 2023. [Online]. Available: https://www.epexspot.com/en

[33] Market Facilitation Forum (MFF) and the Beheerder Afspraken Stelsel (BAS), "mffbas Sectordocuments," 2023. [Online]. Available: https://www.mffbas.nl/en/documents/

[34] C. Van de Veen, "Analysing Thermal Energy Storage in Residential Buildings: Towards Decarbonization of the Heating Sector," Master's thesis, Delft University of Technology, the Netherlands, Oct 2022. [Online]. Available: https://repository.tudelft.nl/islandora/object/uuid:c1fca7b7-a7cb-4ddc-936e-239a8f0a6cb7?collection=education

[35] X. Jin, A. Vora, V. Hoshing, T. Saha, G. Shaver, R. E. García, O. Wasynczuk, and S. Varigonda, "Physically-based reduced-order capacity loss model for graphite anodes in Li-ion battery cells," *Journal of Power Sources*, vol. 342, pp. 750–761, 2 2017. [Online]. Available: https://linkinghub.elsevier.com/retrieve/pii/S037877531631802X

[36] J. M. Reniers, G. Mulder, S. Ober-Blöbaum, and D. A. Howey, "Improving optimal control of grid-connected lithium-ion batteries through more accurate battery and degradation modelling," *Journal of Power Sources*, vol. 379, no. September 2017, pp. 91–102, 3 2018. [Online]. Available: https://www.sciencedirect.com/science/article/abs/pii/S0378775318300041

[37] J. Reniers, "Degradation-aware optimal control of grid-connected lithium-ion batteries," Ph.D. dissertation, University of Oxford, 2020.

[38] J. M. Reniers, G. Mulder, and D. A. Howey, "Unlocking extra value from grid batteries using advanced models," *Journal of Power Sources*, vol. 487, no. December 2020, p. 229355, 3 2021. [Online]. Available: https://www.sciencedirect.com/science/article/abs/pii/S0378775320316438

[39] R. D. Perkins, A. V. Randall, X. Zhang, and G. L. Plett, "Controls oriented reduced order modeling of lithium deposition on overcharge," *Journal of Power Sources*, vol. 209, pp. 318–325, 7

2012. [Online]. Available: https://linkinghub.elsevier.com/retrieve/pii/S0378775312005423